High-Performance Molybdenum Disulfide Field-Effect Transistors with Spin Tunnel Contacts

André Dankert,* Lennart Langouche, Mutta Venkata Kamalakar, and Saroj Prasad Dash*

Department of Microtechnology and Nanoscience, Chalmers University of Technology, SE-41296, Göteborg, Sweden

ABSTRACT Molybdenum disulfide has recently emerged as a promising two-dimensional semiconducting material for nanoelectronic, optoelectronic, and spintronic applications. Here, we investigate the field-effect transistor behavior of MoS_2 with ferromagnetic contacts to explore its potential for spintronics. In such devices, we elucidate that the presence of a large Schottky barrier resistance at the MoS_2/ferromagnet interface is a major obstacle for the electrical spin injection and detection. We circumvent this problem by a reduction in the Schottky barrier height with the introduction of a thin TiO_2 tunnel barrier between the ferromagnet and MoS_2. This results in an enhancement of the transistor on-state current by 2 orders of magnitude and an increment in the field-effect mobility by a factor of 6. Our magnetoresistance calculation reveals that such integration of ferromagnetic tunnel contacts opens up the possibilities for MoS_2-based spintronic devices.

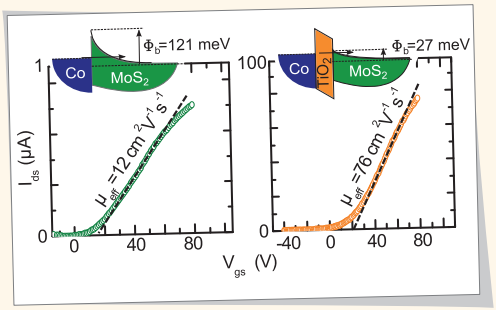

KEYWORDS: MoS_2 · field-effect transistor · ferromagnetic contacts · magnetoresistance · spintronics · Schottky barrier

Two-dimensional (2D) materials are currently explored for their potential role in next-generation nanoelectronic and spintronic devices.[1−4] Graphene has attracted the major attention for its remarkably high electron mobility and long distance spin transport at room temperature.[1,5] However, pristine graphene has neither a band gap nor spin−orbit coupling, which are indispensable requirements for a switching action in charge- or spin-based transistor applications. External doping to engineer a band gap or to induce a spin−orbit coupling in graphene has so far proved detrimental to its intrinsic properties.[6]

Semiconducting molybdenum disulfide (MoS_2) has emerged as a potential alternative 2D crystal demonstrating solutions for several novel nanoelectronic and optoelectronic applications.[7−10] In MoS_2, the lack of inversion symmetry, high atomic mass, and confinement of electron motion in the plane leads to a very strong spin−orbit splitting in the valence band up to 0.3 eV.[9,10] These distinct characteristics lead to the coupling of the spin and valley degrees of freedom, which can only be simultaneously flipped to conserve energy, and therefore provide long spin and valley lifetimes.[10] These spin, orbit, and valley properties are quite unique to MoS_2 and may lead to yet unexplored applications.

For the practical realization of spin-based devices, the electrical injection, transport, manipulation, and detection of spin-polarized carriers in the MoS_2/ferromagnet (FM) heterostructures are primary requirements. However, in such contacts, a Schottky barrier of 100−180 meV is associated with the charge depletion region at the interfaces.[11,12] Therefore, only electrons that are thermally emitted over the Schottky barrier can flow across the contact, resulting in a reduced spin polarization and a low drive current.[13] An even more important concern is the conductivity mismatch between the FM and the MoS_2, which can result in a negligible magnetoresistance (MR).[14,15] Recently, it has been possible to overcome the conductivity mismatch issues for spin injection into semiconductors[16−19] and graphene[20] by employing narrow Schottky barriers or insulating tunnel barriers. For the 2D semiconductor MoS_2, similar approaches

* Address correspondence to andre.dankert@chalmers.se, saroj.dash@chalmers.se.

Received for review September 19, 2013 and accepted December 30, 2013.

Published online December 30, 2013
10.1021/nn404961e

can be explored by using heterostructures with FM tunnel contacts. More recently, a reduction of the Schottky barrier resistance was demonstrated by introducing a MgO tunnel barrier between the FM and single-layer MoS_2.[12] In other studies, it has been shown that a high contact resistance has adverse effects on MoS_2 field-effect transistor (FET) characteristics, reducing the effective mobility (μ_{eff}) and transistor on−off ratio.[11] Additionally, it has also been demonstrated that a maximum mobility of the channel could be achieved by using multilayer (ML) MoS_2 with an optimal thickness of about 10 nm.[11] Such devices also provide larger density of states and multichannel conduction.[21] Therefore, achieving a suitable interface resistance and better transistor properties with FM tunnel contacts in single-layer and ML MoS_2 FETs are the crucial requirements for further developments in spintronic devices.

In this article, we address a major issue related to the electrical spin injection and detection in MoS_2. Our experiments reveal that the presence of a Schottky barrier at the Co/ML MoS_2 interface seriously limits the device performance. We present an approach to engineer the contact resistance by introducing a thin TiO_2 tunnel barrier reducing the Schottky barrier and demonstrating a reduction of the contact resistance and an improved MoS_2 transistor performance. Furthermore, we correlate the contact resistances of our devices with MR calculations on the basis of the spin diffusion model.

RESULTS AND DISCUSSION

MoS_2 flakes were mechanically exfoliated onto a SiO_2/Si substrate. The FM Co electrodes with and without a TiO_2 tunnel barrier were prepared by nanofabrication techniques (see Methods and Figure 1a,b). We used ML MoS_2 with a thickness of about 13 nm (Figure 1c), which promotes a larger density of states and multichannel conduction, allowing for high drive currents.[11,21]

Initially, we studied the two-terminal source−drain current−voltage characteristics (I_{ds}−V_{ds}) of the MoS_2/Co device at zero gate bias (V_{gs} = 0) and room temperature (Figure 1d). The quasi-symmetric nonlinearity of I_{ds}−V_{ds} is due to the back-to-back Schottky diode structures of the devices with a contact resistance area product $R_{cont}A = 3 \times 10^{-7}$ Ωm^2 and a channel resistivity of $\rho = 3 \times 10^{-3}$ Ωm. Such high Schottky barrier and channel resistance of the MoS_2 devices yield problems in spin injection and detection.[13,15] These problems can be resolved by reducing the Schottky barrier and introducing an optimal tunnel barrier resistance.

Next we examine the role of such a TiO_2 tunnel barrier at the interface, which was found to be excellent for spin injection into graphene.[5] The TiO_2 is found to grow homogeneously on MoS_2, without any change in roughness before and after the deposition.

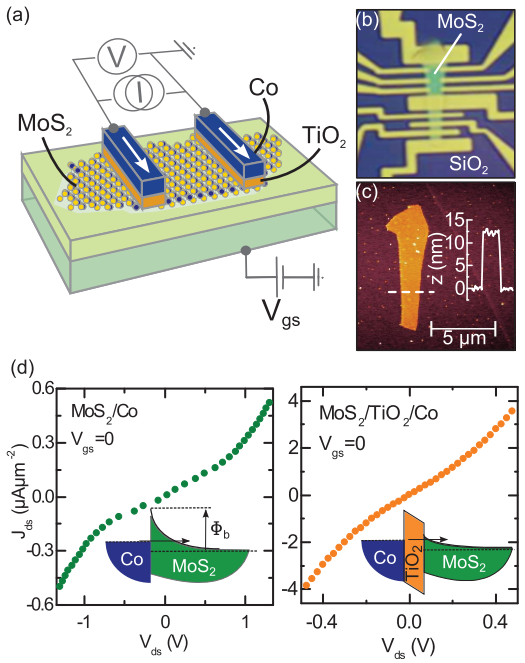

Figure 1. MoS_2 FET with FM contacts. (a) Schematic of a MoS_2 FET with FM tunnel contacts as source and drain and the measurement configuration. (b) Optical image of the fabricated MoS_2 FET with contacts. (c) AFM image and line scan of a 13 nm thin MoS_2 flake exfoliated on SiO_2/n-Si substrate. (d) Current−voltage (I_{ds}−V_{ds}) characteristics of the MoS_2 devices with ferromagnetic source and drain contacts at room temperature and zero gate voltage. Left: MoS_2/Co device; the band diagram demonstrates the Schottky barrier at the interface (inset). Right: MoS_2/TiO_2/Co device; the band diagram depicts a reduction of the Schottky barrier (inset).

The I_{ds}−V_{ds} characteristic of such MoS_2/TiO_2/Co contact also shows a quasi-symmetric nonlinear behavior (Figure 1d). However, the contact resistance is dramatically reduced by 2 orders of magnitude ($R_{cont}A$ = 2.4×10^{-9} Ωm^2) when compared to the direct Co/MoS_2 contact. Such behavior has been reproduced in multiple devices prepared independently. This reduction in contact resistance can be attributed to a lowering of the Schottky barrier height. Similar results were reported with MgO as a tunnel barrier on single-layer MoS_2[12] and in germanium.[22]

In a Co/TiO_2/MoS_2 contact, the Schottky barrier height Φ_b is determined by various parameters, such as the work function of Co (Φ_m), the electron affinity of MoS_2, the thickness and dielectric constant of TiO_2, the charge neutrality level, and the surface density of gap states at the MoS_2 interface.[22−25] Considering that the properties of Co, TiO_2, and MoS_2 are unaffected, the critical parameters which can influence the Schottky barrier are the charge neutrality level and the surface density of gap states at the MoS_2 interface with the preparation of the TiO_2 barrier. The interface gap states can alleviate the Fermi level pinning and result in a lowering of the Schottky barrier height.[11,12,22,25,26]

To understand the modification of the Schottky barrier height, we performed detailed temperature- and

gate-dependent drain−source *IV* characteristics of devices with and without the TiO_2 tunnel barrier (Figure 2).[12] The $I_{ds}-V_{ds}$ characteristics (Figure 2a) show a weak temperature dependence for the $MoS_2/TiO_2/Co$ device compared to the direct Co contact. Such a weak temperature dependence is a manifestation of a reduced Schottky barrier height due to the introduction of the TiO_2 layer. To be noted, to extract the true Schottky barrier values, the $I_{ds}-V_{ds}$ measurements were performed in the flat band condition by applying a gate voltage of V_{gs} = 3 V in the MoS_2/Co and $V_{gs} = -15$ V in the $MoS_2/TiO_2/Co$ device. These flat band voltages, V_{fb}, are obtained from the V_{gs} dependence of the Schottky barrier.[11]

In order to extract the Schottky barrier height at a certain V_{gs}, we employed the three-dimensional thermionic emission equation describing the electrical transport through a Schottky barrier into the ML MoS_2 channel:[11,12,27]

$$I_{ds} = AA^*T^2\exp\left[-\frac{e}{k_BT}\left(\Phi_b - \frac{V_{ds}}{n}\right)\right] \quad (1)$$

where A is the contact area, A^* is the Richardson constant, e is the electron charge, k_B the Boltzmann constant, Φ_b is the Schottky barrier height, and n is the ideality factor. Figure 2b shows the Arrhenius plot ($\ln(I_{ds}T^{-2})$ *versus* T^{-1}) for different bias voltages V_{ds}. The slopes $S(V_{ds})$ extracted from the Arrhenius plot follow a linear dependence with V_{ds} ($S(V_{ds}) = -(e/k_B)(\Phi_b - (V_{ds}/n))$), as displayed in Figure 2c. The Schottky barrier is evaluated from the extrapolated value of the slope at zero drain−source voltage ($S_0 = -(e\Phi_b/k_B)$). We obtained a drastic reduction of the Schottky barrier height Φ_b from 121 meV for the direct Co contact to 27 meV in the $MoS_2/TiO_2/Co$ device calculated at their respective V_{fb}. These flat band voltages were extracted from the gate-voltage-dependent Schottky barrier height plots shown in Figure 2d. For $V_{gs} < V_{fb}$, the thermionic emission dominates the measured current, resulting in a linear dependence of Φ_b on V_{gs}. However, for $V_{gs} > V_{fb}$, the tunnel current through the deformed Schottky barrier starts to contribute increasingly, resulting in a deviation from the linear response.[11] The true Schottky barrier height is obtained from the point of onset of the deviation.

To rule out the presence of metallic Ti in our TiO_2 tunnel barrier and its influence on the reduction of the Schottky barrier, we performed a control experiment with direct Ti/Au contacts (see Supporting Information). The MoS_2/Ti/Au device shows a similar high contact resistance as the Co/MoS_2 devices (Supporting Information Figure S1). The independence of the contact resistance with change in work function of the metals is also evidence of a Fermi level pinning close to the conduction band of the MoS_2.[11] Therefore, this depinning of the Fermi level and the reduction of the contact resistance

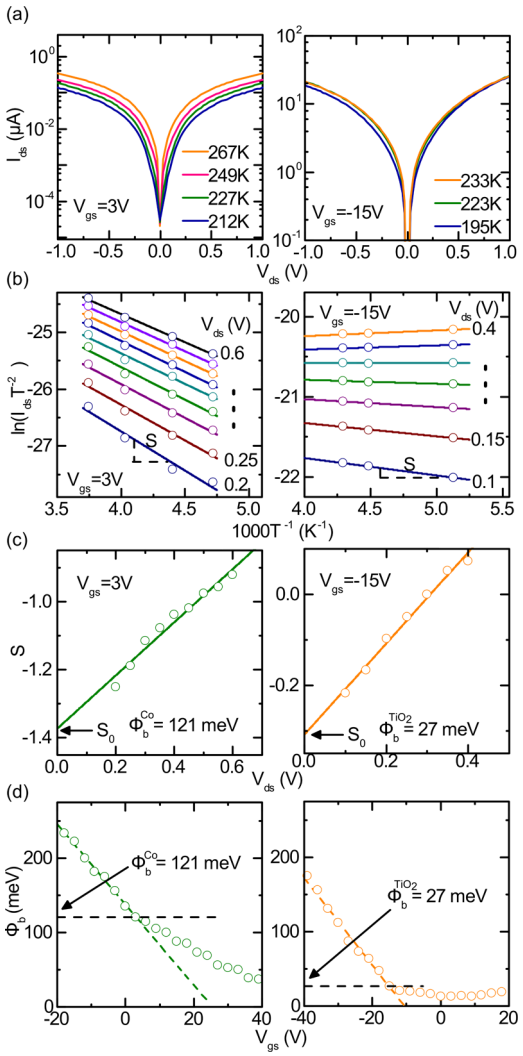

Figure 2. Temperature-dependent measurements and Schottky barrier height. The data presented are for a MoS_2/Co (left panel) and a $MoS_2/TiO_2/Co$ (right panel) contact. (a) $I_{ds}-V_{ds}$ characteristics for temperatures between 194 and 267 K at the flat band voltages. (b) $I_{ds}T^{-2}$ dependence on T^{-1} in an Arrhenius plot with linear fits. (c) Bias voltage dependence of the extracted slope S returns the zero bias slope S_0 to calculate the Schottky barrier height: 121 meV for the MoS_2/Co and 27 meV for the $MoS_2/TiO_2/Co$ contact. (d) Gate-voltage-dependent Schottky barrier height; the deviation from the linear response at low V_{gs} (dotted line) defines the flat band voltage and the real Schottky barrier height.

by introducing a TiO_2 tunnel barrier is extremely promising for electrical spin injection into MoS_2.

Apart from the requirement of an ideal contact resistance for spin injection and detection, it is also very important to achieve higher channel mobilities and better transistor properties for spin transport and especially spin manipulation in MoS_2 devices. Therefore, we investigate the transistor behavior of Co/MoS_2 devices with and without TiO_2 tunnel barriers. The transistor characterization of the devices was performed in a source−drain geometry with an applied gate voltage. Different measurement configurations

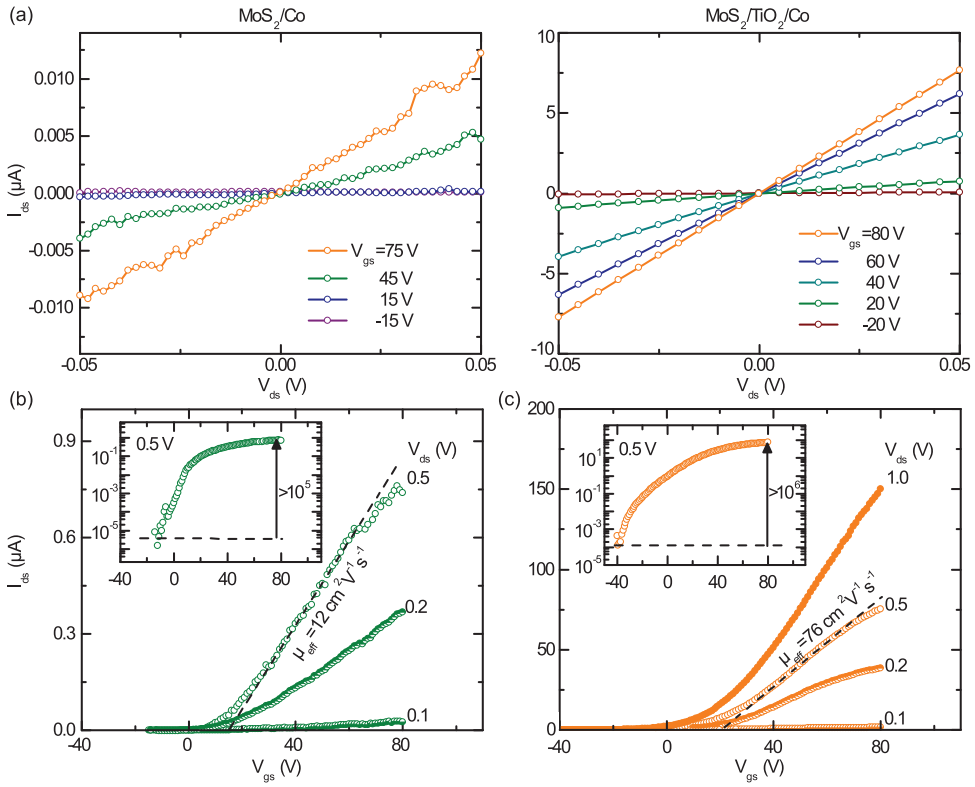

Figure 3. Characterization of MoS_2 FETs. (a) Output characteristics $I_{ds}-V_{ds}$ measured at low bias range for different gate voltages (V_{gs}) for both Co/MoS_2 (left panel) and Co/TiO_2/MoS_2 devices (right panel). (b) Transfer characteristic $I_{ds}-V_{ds}$ for the MoS_2/Co FET with different source−drain bias voltages (V_{ds}) in a linear scaling. An effective field-effect mobility can be extracted from the subthreshold slope ($\mu_{eff} = 12\ cm^2\ V^{-1}\ s^{-1}$). The logarithmical scaling for $V_{ds} = 0.5$ V (inset) reveals a on−off ratio of $I_{on}/I_{off} > 10^5$. (c) Transfer characteristic for the MoS_2/TiO_2/Co FET. The effective field-effect mobility is $\mu_{eff} = 76\ cm^2\ V^{-1}\ s^{-1}$, and $I_{on}/I_{off} > 10^6$ (inset).

were used to determine output and transfer characteristics of the devices. Output characteristics were measured by sweeping the drain−source voltage (V_{ds}), while measuring the drain−source current (I_{ds}) at several gate voltages (V_{gs}) (Figure 3a). The transfer characteristics were recorded by sweeping the V_{gs} while measuring the I_{ds} at different V_{ds} at room temperature (Figure 3b,c). The output characteristics of both devices show a linear $I_{ds}-V_{ds}$ behavior at small bias voltages (Figure 3a). However, such behavior does not necessarily indicate an Ohmic contact as perceived previously.[8] Thermally assisted tunneling in nanolayers of MoS_2 at finite temperatures can cause a linear dependence despite the presence of a sizable Schottky barrier at the MoS_2/Co interface. As we discussed previously, the Schottky barrier and the carrier depletion at the interfaces give rise to higher contact resistances and nonlinear $I_{ds}-V_{ds}$ characteristics at high voltages. Introducing a TiO_2 tunnel barrier between the Co and MoS_2 lowers the contact resistance by 2−3 orders of magnitude (Figure 1d). The decrease in contact resistance with the TiO_2/Co contact also results in an improved transistor performance. The measured transfer characteristics are typical for n-type FET devices, which is determined by the position of the Co Fermi level close to the conduction band of the MoS_2. The high contact resistance in the Co/MoS_2 device limits the drive current to about 4 $\mu A/\mu m^{-2}$ and results in the low transistor performance (Figure 3b). The introduction of TiO_2 leads to a high saturation current density up to 560 $\mu A/\mu m^{-2}$ with a carrier concentration of 9×10^{12} cm^{-2}, making the device characteristics even more favorable for spin transport (Figure 3c).

Furthermore, the ferromagnetic tunnel contact MoS_2/TiO_2/Co also showed a significant enhancement in field-effect mobility and transistor on−off ratio. The effective field-effect mobility is estimated by extracting the subthreshold slope dI_{ds}/dV_{gs} from the transfer characteristics (Figure 3a):

$$\mu_{eff} = \frac{dI_{ds}}{dV_{gs}} \frac{L}{wC_iV_{ds}} \quad (2)$$

where L is the length, w is the width of the channel, and C_i is the gate capacitance.[8] The effective field-effect mobility is found to be $\mu_{eff} = 12\ cm^2\ V^{-1}\ s^{-1}$ for the MoS_2/Co device (Figure 3b). This value is comparable to previously reported mobilities for ML MoS_2 on SiO_2 substrates without using any high-k dielectric capping layer.[11,28] In contrast, the devices with TiO_2 exhibits a much higher mobility of $\mu_{eff} = 76\ cm^2\ V^{-1}\ s^{-1}$ (Figure 3c). This demonstrates that the introduction of a TiO_2 tunnel barrier reduces the contact resistance

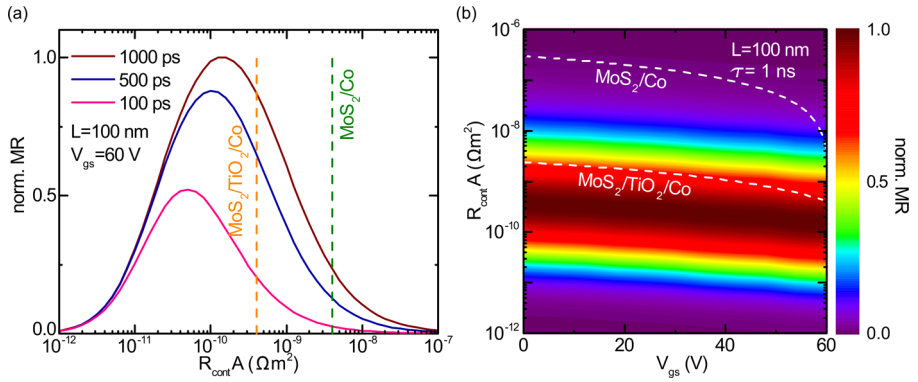

Figure 4. Contact resistance for observation of MR. Calculated MR of FM/I/MoS_2/I/FM spin FET structure as a function of the contact resistance area product ($R_{cont}A$) for a channel length of 100 nm at room temperature. The values are normalized to the peak value at a spin lifetime τ_{sf} = 1 ns. (a) Calculation for different spin lifetimes τ_{sf} at a gate voltage V_{gs} = 60 V (on-state). The vertical lines represent the $R_{cont}A$ value for the TiO_2/Co tunnel and the direct Co contact on MoS_2 in our experiments. (b) MR as a function of gate voltage and contact resistance. The dashed lines represent the variation of contact *RA* of our devices with gate voltage.

and increases the effective field-effect mobility by a factor of 6. Furthermore, the MoS_2 devices with direct Co contact show a current on−off ratio of $I_{on}/I_{off} > 10^5$, whereas a device with TiO_2/Co contact exhibits a drastic increase in $I_{on}/I_{off} > 10^6$. These results clearly indicate the requirement of lower contact resistance to extract intrinsic device parameters of MoS_2.[29]

In order to understand the viability of ferromagnetic tunnel contacts on MoS_2 for the observation of two-terminal MR, we put the contact resistances in our devices into perspective with the spin diffusion theory.[14,30] We consider a FM/I/MoS_2/I/FM structure, where I is the interface contact. By taking experimentally measured mobility and resistances into account, we estimate the optimal contact resistance. To observe a high MR, the interface resistance should lie within the range

$$\rho_N L < R_{cont}A < \frac{\rho_N l_{sf}^2}{L} \qquad (3)$$

where ρ_N is the resistivity of the MoS_2 channel, R_{cont} is the contact resistance, A is the contact area, l_{sf} is the spin diffusion length, and L is the channel length in the MoS_2.[14] Figure 4a shows the calculated MR as a function of contact resistance area product ($R_{cont}A$) for the channel length of L = 100 nm and different expected spin lifetimes in MoS_2. The latter is a relevant factor to consider because the experimentally observed lifetime could be well below the theoretical prediction of τ_{sf} = 1 ns.[10] This calculation shows the possibility of observation of a significant MR in a narrow contact resistance range. The low MR for small contact resistances is due to the conductivity mismatch, preventing a spin injection from the Co contact into MoS_2. The decay of the MR for larger resistances is caused by the relaxation of the spins during the time spent in the MoS_2 channel.[14]

For our MoS_2/Co device, the contact resistance is very high ($R_{cont}A = 4 \times 10^{-9}$ Ωm^2 in FET on-state with V_{gs} = 60 V) and lies in the higher end of the resistance window corresponding to the low MR region (Figure 4a). In contrast, by introducing a thin TiO_2 tunnel barrier, we dramatically reduce the contact resistance ($R_{cont}A = 4 \times 10^{-10}$ Ωm^2) to the optimum range for the observation of a large MR. Furthermore, we show the calculated MR as a function of gate voltage V_{gs} and contact resistance $R_{cont}A$ in Figure 4b. The observed shift in MR is because of the tuning of the carrier density in the MoS_2 channel by the gate voltage. In addition, the change in contact resistance of our devices (dashed lines in Figure 4a) is due to deformation of the Schottky barrier. Notably, the reduced Schottky barrier height for the MoS_2/TiO_2/Co contact results in a weaker V_{gs} dependence compared to the direct Co contact. Our results demonstrate the tunability of the channel, contact, and MR by the gate voltage. In addition to the improved transistor performance, the TiO_2/Co spin tunnel contacts are in the optimum range for spin injection and detection in MoS_2 over the full gate voltage range. Further enhancements in the MR can be achieved by improving the mobility of the MoS_2 channel. Such improvements in mobility can be realized by recently demonstrated techniques, such as encapsulating MoS_2 structures in high-k dielectrics[21,28] or atomically flat hexagonal boron nitride.[31,32] This allows not only to explore spin-transistor-based devices but also to detect spin currents in MoS_2 created by spin Hall effect and other spin-related phenomena.

CONCLUSION

In conclusion, we presented an improved field-effect transistor behavior of MoS_2 with ferromagnetic tunnel contacts. The higher contact resistance and limited transistor performance of direct Co contacts on MoS_2 could be circumvented by introducing a TiO_2 tunnel barrier. We demonstrated a drastic reduction of the contact resistance, which resulted in an increase in the transistor on-state current by 2 orders of magnitude

reaching 560 $\mu A \mu m^{-2}$ and the effective field-effect channel mobility by a factor of 6. Our calculations for the observation of two-terminal MR indicate that the implementation of TiO_2 has many advantages to develop efficient spintronic devices based on MoS_2. The integration of such ferromagnetic tunnel contacts on MoS_2 bypasses the conductivity mismatch problem and improves the transistor performance. Furthermore, the channel conductance, contact resistance, and expected MR can be tuned by an applied gate voltage. This offers a multitude of possibilities to combine spintronic effects with regular electronics.

METHODS

The MoS_2 flakes were exfoliated from a bulk crystal (SPI Supplies), using the conventional cleavage technique, onto a clean SiO_2 (285 nm)/highly doped n-type Si substrate. The flakes were identified using a combination of optical (Figure 1b) and atomic force microscopy (Figure 1c). We used multilayer MoS_2 with a thickness of about 13 nm and widths of $1-2\ \mu m$. The SiO_2/n-Si is used as a gate to control the carrier concentration in the MoS_2. Contacts of Co (65 nm)/Au (20 nm) were prepared on the MoS_2 samples by electron beam lithography, electron beam evaporation, and lift-off technique. Electrodes with widths of $0.5-1\ \mu m$ and channel lengths of $0.5-1\ \mu m$ are used. The 1 nm TiO_2 tunnel barrier was deposited by sputtering technique. Using a dc argon/oxygen plasma with a Ti source results in a TiO_2 deposited on the target. Afterward, the sample transferred into an electron beam evaporation system to deposit the Co (65 nm)/Au (20 nm) contacts.

Conflict of Interest: The authors declare no competing financial interest.

Acknowledgment. The authors acknowledge the support of colleagues at the Quantum Device Physics Laboratory and Nanofabrication Laboratory at Chalmers University of Technology. The authors would also like to acknowledge the financial supported from the Nano Area of the Advance program at Chalmers University of Technology.

Supporting Information Available: MoS_2 FET characteristics with Ti/Au contacts without TiO_2 tunnel barrier. This material is available free of charge *via* the Internet at http://pubs.acs.org.

REFERENCES AND NOTES

1. Geim, A. K.; Grigorieva, I. V. van der Waals Heterostructures. *Nature* **2013**, *499*, 419–425.
2. Novoselov, K. S.; Fal, V.; Colombo, L. A Roadmap for Graphene. *Nature* **2012**, *490*, 192–200.
3. Tombros, N.; Jozsa, C.; Popinciuc, M.; Jonkman, H. T.; van Wees, B. J. Electronic Spin Transport and Spin Precession in Single Graphene Layers at Room Temperature. *Nature* **2007**, *448*, 571–574.
4. Dlubak, B.; Martin, M. B.; Deranlot, C.; Servet, B.; Xavier, S.; Mattana, R.; Sprinkle, M.; Berger, C.; De Heer, W. A.; Petroff, F.; *et al.* Highly Efficient Spin Transport in Epitaxial Graphene on SiC. *Nat. Phys.* **2012**, *8*, 557–561.
5. Zomer, P.; Guimarães, M.; Tombros, N.; van Wees, B. J. Long-Distance Spin Transport in High-Mobility Graphene on Hexagonal Boron Nitride. *Phys. Rev. B* **2012**, *86*, 161416.
6. Li, X.; Wang, X.; Zhang, L.; Lee, S.; Dai, H. Chemically Derived, Ultrasmooth Graphene Nanoribbon Semiconductors. *Science* **2008**, *319*, 1229–1232.
7. Mak, K. F.; Lee, C.; Hone, J.; Shan, J.; Heinz, T. F. Atomically Thin MoS_2: A New Direct-Gap Semiconductor. *Phys. Rev. Lett.* **2010**, *105*, 136805.
8. Radisavljevic, B.; Radenovic, A.; Brivio, J.; Giacometti, V.; Kis, A. Single-Layer MoS_2 Transistors. *Nat. Nanotechnol.* **2011**, *6*, 147–150.
9. Xiao, D.; Liu, G. G. B.; Feng, W.; Xu, X.; Yao, W. Coupled Spin and Valley Physics in Monolayers of MoS_2 and Other Group-VI Dichalcogenides. *Phys. Rev. Lett.* **2012**, *108*, 196802.
10. Mak, K. F.; He, K.; Shan, J.; Heinz, T. F. Control of Valley Polarization in Monolayer MoS_2 by Optical Helicity. *Nat. Nanotechnol.* **2012**, *7*, 494–498.
11. Das, S.; Chen, H. Y.; Penumatcha, A. V.; Appenzeller, J. High Performance Multilayer MoS_2 Transistors with Scandium Contacts. *Nano Lett.* **2013**, *13*, 100–105.
12. Chen, J. R.; Odenthal, P. M. P.; Swartz, A.; Floyd, G. C. G.; Wen, H.; Luo, K. Y.; Kawakami, R. K. Control of Schottky Barriers in Single Layer MoS_2 Transistors with Ferromagnetic Contacts. *Nano Lett.* **2013**, *13*, 3106–3110.
13. Jansen, R.; Min, B. C. Detection of a Spin Accumulation in Nondegenerate Semiconductors. *Phys. Rev. Lett.* **2007**, *99*, 246604.
14. Fert, A.; Jaffrès, H. Conditions for Efficient Spin Injection from a Ferromagnetic Metal into a Semiconductor. *Phys. Rev. B* **2001**, *64*, 184420.
15. Schmidt, G.; Ferrand, D.; Molenkamp, L.; Filip, A.; van Wees, B. J. Fundamental Obstacle for Electrical Spin Injection from a Ferromagnetic Metal into a Diffusive Semiconductor. *Phys. Rev. B* **2000**, *62*, R4790–R4793.
16. Lou, X.; Adelmann, C.; Crooker, S. A.; Garlid, E. S.; Zhang, J.; Reddy, K. S. M.; Flexner, S. D.; Palmstrøm, C. J.; Crowell, P. A. Electrical Detection of Spin Transport in Lateral Ferromagnet-Semiconductor Devices. *Nat. Phys.* **2007**, *3*, 197–202.
17. Dash, S. P.; Sharma, S.; Patel, R. S.; de Jong, M. P.; Jansen, R. Electrical Creation of Spin Polarization in Silicon at Room Temperature. *Nature* **2009**, *462*, 491–494.
18. Dankert, A.; Dulal, R. S.; Dash, S. P. Efficient Spin Injection into Silicon and the Role of the Schottky Barrier. *Sci. Rep.* **2013**, *3*, 3196.
19. Dankert, A.; Dash, S. P. Thermal Creation of Electron Spin Polarization in n-Type Silicon. *Appl. Phys. Lett.* **2013**, *103*, 242405.
20. Han, W.; Wang, W.; Pi, K.; McCreary, K.; Bao, W.; Li, Y.; Miao, F.; Lau, C.; Kawakami, R. Electron-Hole Asymmetry of Spin Injection and Transport in Single-Layer Graphene. *Phys. Rev. Lett.* **2009**, *102*, 137205.
21. Kim, S.; Konar, A.; Hwang, W. S.; Lee, J. H.; Yang, J.; Jung, C.; Kim, H.; Yoo, J. B.; Choi, J. Y.; Jin, Y. W.; *et al.* High-Mobility and Low-Power Thin-Film Transistors Based on Multilayer MoS_2 Crystals. *Nat. Commun.* **2012**, *3*, 1011.
22. Lin, J. Y. J.; Roy, A. M.; Nainani, A.; Sun, Y.; Saraswat, K. C. Increase in Current Density for Metal Contacts to N-Germanium by Inserting TiO_2 Interfacial Layer To Reduce Schottky Barrier Height. *Appl. Phys. Lett.* **2011**, *98*, 092113.
23. Bardeen, J. Surface States and Rectification at a Metal Semi-conductor Contact. *Phys. Rev.* **1947**, *71*, 717–727.
24. Tung, R. T. Chemical Bonding and Fermi Level Pinning at Metal-Semiconductor Interfaces. *Phys. Rev. Lett.* **2000**, *84*, 6078–6081.
25. Zhou, Y.; Han, W.; Wang, Y.; Xiu, F.; Zou, J.; Kawakami, R. K.; Wang, K. L. Investigating the Origin of Fermi Level Pinning in Ge Schottky Junctions Using Epitaxially Grown Ultrathin MgO Films. *Appl. Phys. Lett.* **2010**, *96*, 102103.
26. Jansen, R.; Min, B. C.; Dash, S. P.; Sharma, S.; Kioseoglou, G.; Hanbicki, A. T.; van't Erve, O. M. J.; Thompson, P. E.; Jonker, B. T. Electrical Spin Injection into Moderately Doped Silicon Enabled by Tailored Interfaces. *Phys. Rev. B* **2010**, *82*, 241305.
27. Sze, S.; Ng, K. *Physics of Semiconductor Devices*; John Wiley & Sons, Inc.: New York, 2006.
28. Radisavljevic, B.; Kis, A. Mobility Engineering and Metal-Insulator Transition in Monolayer MoS_2. *Nat. Mater.* **2013**, *12*, 815–820.

29. Reese, C.; Bao, Z. Overestimation of the Field-Effect Mobility *via* Transconductance Measurements and the Origin of the Output/Transfer Characteristic Discrepancy in Organic Field-Effect Transistors. *J. Appl. Phys.* **2009**, *105*, 024506.
30. Min, B. C.; Motohashi, K.; Lodder, C.; Jansen, R. Tunable Spin-Tunnel Contacts to Silicon Using Low-Work-Function Ferromagnets. *Nat. Mater.* **2006**, *5*, 817–22.
31. Lee, G.; Yu, Y.; Cui, X.; Petrone, N.; Lee, C. Flexible and Transparent MoS_2 Field-Effect Transistors on Hexagonal Boron Nitride-Graphene Heterostructures. *ACS Nano* **2013**, *7*, 7931–7936.
32. Baugher, B. W. H.; Churchill, H. O. H.; Yang, Y.; Jarillo-Herrero, P. Intrinsic Electronic Transport Properties of High-Quality Monolayer and Bilayer MoS_2. *Nano Lett.* **2013**, *13*, 4212–4216.